PAPER

Check for updates

Rapid degradation behavior of encapsulated perovskite solar cells under light, bias voltage or heat fields†

Xiaobo Zhang, [ID] [a] Xiaoqing Chen, [ID] *[b] Yichuan Chen,[a] Nabonswende Aida Nadege Ouedraogo,[a] Jingjie Li,[a] Xiulong Bao,[c] Chang Bao Han, [ID] [a] Yasuhiro Shirai, [ID] [d] Yongzhe Zhang [ID] *[b] and Hui Yan[a]

When the power conversion efficiency (PCE) of perovskite solar cells (PSCs) rapidly approaches that of commercial solar cells, the stability becomes the most important obstacle for the commercialization of PSCs. Aside from the widely studied slow PCE degradation, the PSCs also show a unique rapid PCE degradation. Although the degradation due to oxygen and humidity can be avoided by encapsulation, that due to bias voltage, light and heat could not be effective suppressed and will lead to considerable degradation. Usually, the rapid PCE degradation is believed to be from ion migration. However, a systematic investigation is yet to be carried out. This work quantitatively and systematically investigated the relationships between external fields (bias voltage, light or heat), ion migration and device performance. By comparing the performance of reference PSCs after 90 min degradation under these fields, we conclude that (1) the electric field affects the spatial distribution of mobile ions; (2) the light field changes the mobile ion densities and drives the ion migration; (3) the heat field results in perovskite decomposition as well as changing the mobile ion densities. In addition to the analysis of the reference device, we experimentally proved that the improved device stability upon introducing phenethylammonium iodide (PEAI) or poly-methyl methacrylate (PMMA) layers originates from the inhibition of mobile ion density and migration.

1. Introduction

With power conversion efficiency (PCE) beyond 25% which is comparable to that of commercial solar cells, organic–inorganic hybrid perovskite solar cells (PSCs) have attracted intense interest in solar energy utilization. Despite the rapid development in efficiency, the commercialization of perovskite solar cells is still limited by the device stability.[1,2] The degradation of PSCs briefly includes a rapid PCE degradation (<5 h) which is often reversible and a slow PCE degradation (>5 h) which is irreversible.[3] Usually, stability studies of PSCs focus on the slow PCE degradation. However, although the rapid PCE degradation is reversible, it still results in *ca.* 30% PCE loss when the PSCs

are employed in practical power plants.[3,4] The behavior and degradation mechanism of the rapid PCE degradation is fundamentally different from the slow one both in timescale and in reversibility. This is probably because the initial rapid PCE degradation process mainly stems from the migration of organic cations,[3,5] while the slow PCE degradation mainly stems from material decomposition.[2,6,7] Reported reasons for degradation of device performance include light, temperature, bias voltage, oxygen, and humidity. Although the degradation due to oxygen and humidity can be avoided by encapsulation, that due to external fields (including bias voltage, light and heat) could not be effectively suppressed and will lead to considerable degradation.[9–11] Because the degradation under the different external field conditions cannot be solved by encapsulation and the degradation mechanism under different external field conditions is complex and unclear, investigating the degradation process of encapsulated devices under bias voltage, light and heat conditions is particularly important for the PSCs' commercial application. In this paper, we will systematically study the relationship between external fields, ion migration and device degradation. The field-assisted ion migration, which has been confirmed by *in situ* SEM, AFM, PL, *etc.*,[12–15] can lead to perovskite phase segregation, ion accumulation at the interface and tuning of the band energy diagram. However, we still need

[a]Faculty of Materials and Manufacturing, Beijing University of Technology, Beijing 100124, China

[b]Key Laboratory of Optoelectronics Technology, Ministry of Education, Faculty of Information Technology, Beijing University of Technology, Beijing 100124, China. E-mail: chenxiaoqing@bjut.edu.cn; yzzhang@bjut.edu.cn

[c]School of Electrical and Electronic Engineering, Beijing-Dublin International College (BDIC), University College Dublin, Ireland

[d]National Institute for Materials Science (NIMS), 1-1 Namiki, Tsukuba, Ibaraki, 305-0044, Japan

† Electronic supplementary information (ESI) available. See DOI: 10.1039/d1na00495f

a systematic and quantitative study to clarify the relationship between the external field, ion migration and device performance which is necessary for PSCs.

Recently, various passivation materials have been reported to be capable of suppressing the ion migration and consequently the rapid PCE degradation. The passivation materials include low dimensional perovskites (*e.g.* PEAI)[16–19] and organic polymer layers (*e.g.* PMMA).[20,21] Meanwhile, these two passivation materials are believed to effectively suppress oxygen and humidity induced perovskite decomposition.[19,21] However, at present, work on these materials mainly involves phenomenological research on device performance. To further understand the mechanism of the stability improvement, we need to quantitatively investigate the dynamic evolution of the device performance and the behavior of mobile ions under the external fields with or without the passivation layer. In addition, we need to study the impacts of ions on free carrier migration and device performance, namely, (1) the static ions in the perovskite bulk are dopants that influence the free carrier lifetime and (2) the accumulation of the mobile ions near the perovskite interface which suppresses the device's built-in electric field. Therefore, we employed two methods under various external fields, (1) the capacitance–voltage Mott–Schottky relationship (M–S) which is the classical tool to analyze the semiconductor doping concentration and built-in electric field,[22] and (2) electrochemical impedance spectroscopy (EIS), which is widely used in analyzing the free carrier lifetime and ion migration.[23–25]

2. Results and discussion

2.1. Performance of the as-prepared devices

A schematic of the involved planar PSCs is shown in Fig. 1, including the ITO/SnO$_2$/FA$_x$MA$_{1-x}$PbI$_y$Cl$_{1-y}$/passivation layer/Spiro-OMeTAD/Au (with the experimental details given in the ESI†). Three types of device are involved in this study, namely, (1) the reference devices without an interface passivation layer, (2) the PEAI devices with PEAI passivation and (3) the PMMA devices with PMMA passivation. As shown by the *J–V* curves in Fig. S2a,† before degradation, the PCE of the champion reference device is 18.8%, which is similar to the reported values.[17,26,27] After the introduction of PMMA or PEAI, the PCE increased to 20.2% and 19.8%, respectively, which is further confirmed by the statistical PCE values shown in Fig. S2b.† This

PCE improvement stems from the interface passivation of the PSCs.[17,18] To further clarify the reasons for the PCE improvement, other device performance characteristics (spectroscopic EQE, light absorption, dependence of V_{oc} on light intensity, space-charge-limited current of the champion devices and the statistical hysteresis index) have been investigated and the results are shown in Fig. S4.† As mentioned in the introduction, the device degradation is apparently divided in two stages as shown in Fig. S5,† (1) the rapid PCE degradation stage and (2) the slow PCE degradation stage. We find that only the initial rapid decay (<90 min) is a reversible degradation process, which is related to ion migration in the perovskite layer. After 90 min light soaking treatment (Fig. S5†), the PCE degradation occurs in a very slow and irreversible degradation stage, which involves the failure of the functional layer (for example, materials decomposition or mobile ion migration into the charge transport layer/metal electrode layer).[3,8,28,29] Halide ion migration induced hysteresis (timescale from 10^{-1} to 10^2 s) and materials decomposition induced PCE irreversible degradation (timescale above 5 h) have been widely studied.[15,30–37] However, some mechanisms of this rapid PCE degradation behavior (timescale from 10^2 s to 5 h) still remain unclear. Therefore, this paper only focuses on the dynamic process of the reversible and rapid decay stage and thus the selected aging time of the device is within 90 min.

In the following sections, we consecutively discuss the degradation induced by a bias voltage, light or heat field. To eliminate the effects of water and oxygen, all devices were encapsulated using glass and epoxy resin. The bias voltage aging process was measured under 1 V under dark conditions and at controlled temperature (25 °C). The entire light aging process was measured using an AM1.5 solar simulator under open circuit conditions and at controlled temperature (25 °C). The heat aging process was measured at controlled temperature (85 °C) under dark conditions. Under the abovementioned aging conditions, the corresponding results of the device performance degradation or kinetic process are discussed in the following sections.

2.2. Voltage-induced rapid degradation

The fast PCE degradation of the encapsulated device in the dark under 1 V is studied. A 1 V bias was applied in the voltage-aging test because the goal of this experiment was to study the effect of 1 V bias on device degradation. However, the 1 V bias can affect the device performance during the measurements. Therefore, no DC bias was applied in the following light-aging and heat-aging tests. In these two experiments, only 10 mV perturbation voltage was applied to the devices. We believe that the perturbation voltage would not lead to significant degradation because its amplitude was negligible compared to the 1 V DC bias and it was applied only for *ca.* 1 min during each measurement. As shown in Fig. 2, the modified cells have a much better voltage-stability than the reference devices. Using the PEAI or PMMA device, the efficiency can conserve up to 90% of the initial value after 90 min continuous bias voltage application. The reference device has the worst stability, retaining
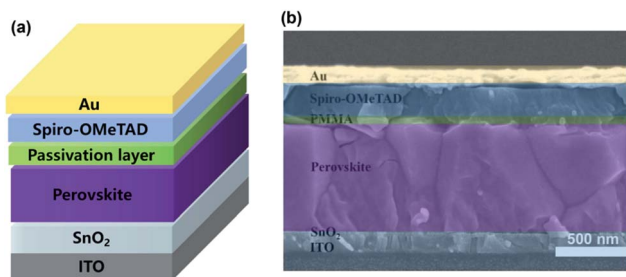

Fig. 1 (a) Architecture of a planar perovskite solar cell fabricated with the two-step deposition method. (b) Cross-sectional SEM images of the PMMA device.
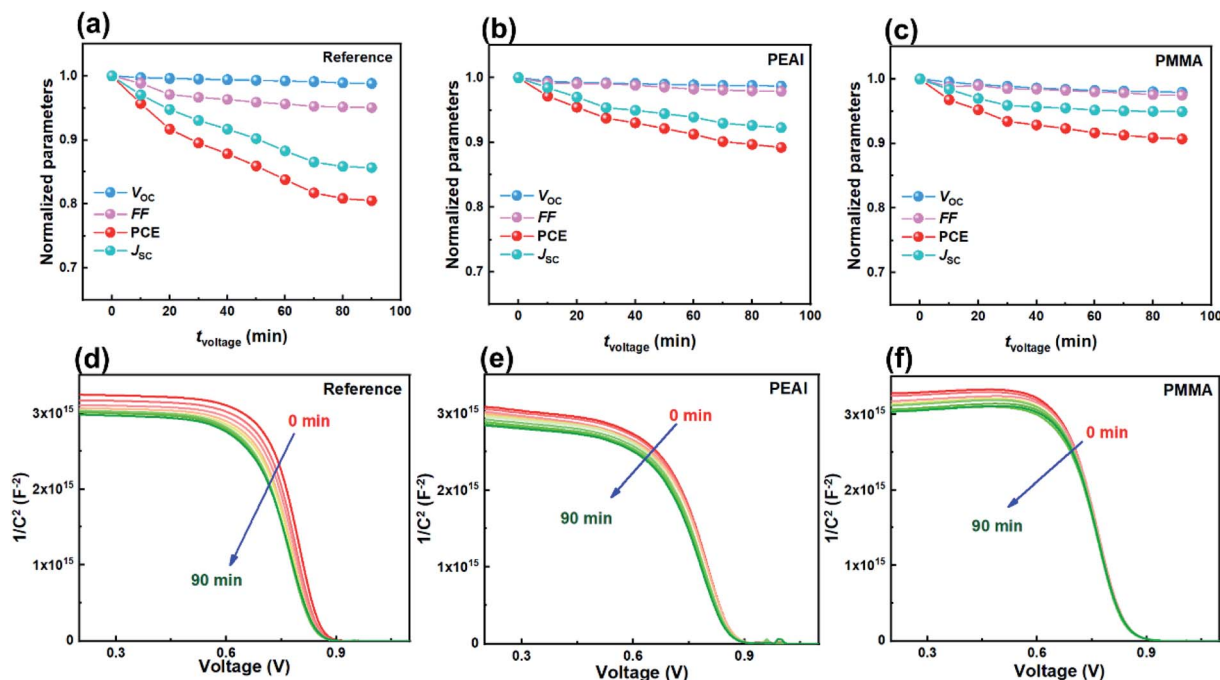
Fig. 2 Bias voltage-induced rapid degradation behavior of performance parameters of the encapsulated reference device (a), PEAI device (b) and PMMA device (c) with $t_{voltage}$, in the air at 25 °C. M–S plots of the degradation process over $t_{voltage}$ of the reference device (d), PEAI device (e) and PMMA device (f) measured at 1 kHz and in the dark.

only 80.4% of its original value. The decrease of J_{sc} is the most significant (85.6%) while the V_{oc} and FF retained 98.8% and 95.1% of their initial values. To investigate the evolution of bulk doping density (N) and the built-in field (V_{bi}) throughout the voltage-induced rapid degradation, M–S measurement results (capacitance–voltage relationship) measured in the dark (Fig. 2d–f) are analyzed according to the Mott–Schottky relationship,[22]

$$\frac{1}{C^2} = \frac{2(V_{bi} - V_{app})}{A^2 N \varepsilon_0 \varepsilon_r q} \quad (1)$$

where V_{app}, A, ε_r, ε_0, and q are the applied voltage, active area of the device, relative permittivity of the perovskite, vacuum permittivity and elementary charge, respectively. Two issues should be noted when using the Mott–Schottky relationship. First, the depletion region width must be smaller than the perovskite layer thickness, which is 800 nm in this work. This criterion requires that the doping density be larger than a specific value introduced by Ravishankar et al.[38] Under our conditions, the minimum doping density is calculated to be ca. 8×10^{14} cm^{-3}. Otherwise, the effect from geometric and injection capacitances will overtake the contribution from the depletion region. Next, the calculated apparent doping density in the bulk is a statistical value for the entire perovskite layer, which corresponds to the linear apparent Mott–Schottky regime.[38] More details of the validation and prerequisites for using the M–S analysis are given in the ESI.†

According to calculation, after the 90 min voltage-induced rapid degradation, N values of the reference, PEAI and PMMA devices increased from 1.29×10^{16} cm^{-3} to 1.63×10^{16} (26.4%↑),

from 1.76×10^{16} to 1.98×10^{16} (12.5%↑) and from 1.37×10^{16} cm^{-3} to 1.48×10^{16} cm^{-3} (8.0%↑), respectively. Namely, N of both modified devices barely changed, implying that the passivation layer can effectively inhibit the voltage-induced doping density increase in the perovskite bulk. This can be attributed to the fact that PEAI and PMMA surface treatments can suppress the formation of charged defects at grain boundaries and surfaces. For example, (1) the π-conjugation structure of the benzene ring of PEAI reduces the neutral iodine related defects; (2) the amine group of PEAI and methyl group of PMMA form a hydrogen bond with the iodide ion and coordinate with the Pb^{2+} interstitials; and (3) the iodide ions of PEAI fill the iodine vacancies.[17,29,39] Simultaneously, the V_{bi} decreases by 31 mV for the reference devices (from 0.872 to 0.841 V) while it stays almost unchanged for the PMMA and the PEAI devices which agrees with their stable V_{oc} shown in Fig. 2b and c. The apparent inhibition of V_{bi} and V_{oc} degradation by interface passivation indicates that the V_{oc} degradation of the reference device stems from the interface at the perovskite/charge transport layer, as confirmed by the following discussion based on the EIS results.

As shown in Fig. 3, the evolution of the EIS results in the Nyquist plots of the reference (a), PEAI (b) and PMMA (c) devices with increasing bias voltage time ($t_{voltage}$) under the dark and 1 V conditions is characterized. Each Nyquist plot consists of two obvious features which could be analyzed according to the model and equivalent circuit proposed in previous literature (Fig. 3d).[40] In this model, (1) the feature at higher frequency is an arc dominated by free carrier recombination, and (2) the feature at lower frequency is dominated by ion migration which could be modeled with a Warburg element (Z_W)[23,40]
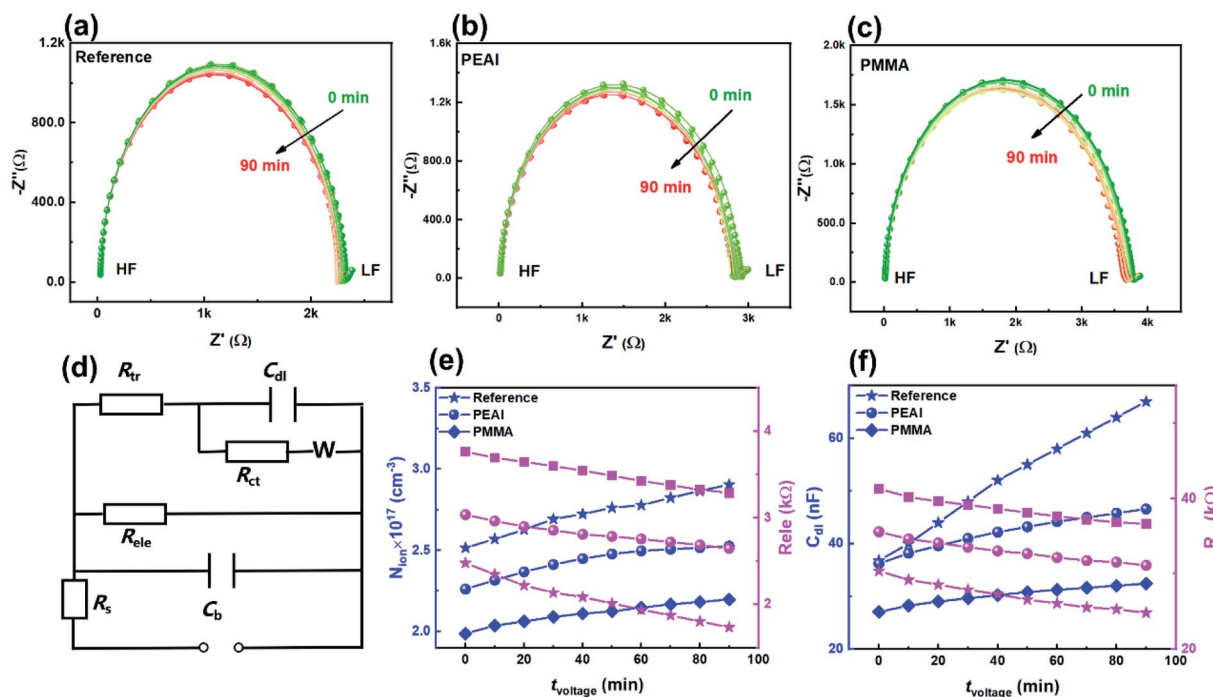
Fig. 3 Nyquist plots of three devices with the bias voltage time ((a) for reference, (b) for PEAI and (c) for PMMA devices). The EIS were measured under a 1 V bias under dark conditions and at controlled temperature (25 °C). The symbols and solid lines represent the experiment data points and fitting curves, respectively. (d) Equivalent circuit diagram used in this work, along with the fitted (e) N_{ion} and R_{ele}, and (f) C_{dl} and R_{ct} of the equivalent circuit components with $t_{voltage}$.

$$Z_W = \frac{A_W}{(i\omega)^{1/2}} \tanh\left((i\omega\tau)^{\frac{1}{2}}\right) \approx A_W(i\omega)^{-\frac{1}{2}} \quad (2)$$

where A_W, τ, and ω represent the Warburg coefficient, the Warburg time constant and angular frequency, respectively. Among these parameters, A_W is determined by the mobile ion density (N_{ion}) and ion diffusion coefficient (D, which is 1.6×10^{-9} cm^2 s^{-1} according to a previous report[23]) according to[23,40]

$$A_W = \frac{k_B T}{A\nu^2 q^2} \frac{1}{N_{ion}\sqrt{D}} \quad (3)$$

where k_B, T, and ν are the Boltzmann constant, temperature, and charge transfer valency ($\nu = 1$ for I$^-$). In this equivalent circuit, C_{dl} is the capacitance of the electric double layer that describes the electronic and ionic charge accumulation at the interfaces (perovskite/electron transport layer, ETL and perovskite/hole transport layer, HTL). C_b is the bulk capacitance element of the depletion width determined by static ion dopants distributed in the perovskite depletion region. R_{tr} is the bulk charge transport resistance. R_{ct} is the interfacial recombination resistance, which relates to mobile ions. The recombination of the free electrons and holes is modeled using another resistance term (R_{ele}). Series resistance (R_s) represents contact resistance, contributed by circuit imperfections during the measurement process.[40]

According to Fig. 3a–c, during the voltage aging test, the time constants of the resonance peaks stayed almost unchanged (~10 μs) for all three devices (Fig. S6†), indicating that the free carrier recombination inside the perovskite bulk is unchanged. This agrees with the almost unchanged N and FF.[37] Different from the unchanged time constant, N_{ion} shows a moderate increase (Fig. 3e) while C_{dl} increases the most (Fig. 3f), according to the calculation based on the equivalent circuit fitting and eqn (2) and (3). The significant increase of C_{dl} indicates the serious accumulation of the mobile ions near the perovskite/charge transport layer interface.[40,41] Previous studies showed that the accumulated mobile ions can capture free carriers,[42,43] as proved by the significant R_{ct} reduction of the reference device (Fig. 3f). The evolutions of N_{ion}, C_{dl} and R_{ct} are more obvious in the reference devices than in the passivated devices. In particular, C_{dl} of the reference device increased by 82.1% which should be responsible for the J_{sc} loss shown in Fig. 2. In contrast, when the devices are passivated by PEAI or PMMA, C_{dl} increased by only 28.7% and 20.1%, respectively. According to the above discussion, we conclude that bias voltage mainly affects the interfacial capacitance C_{dl} (namely, changes the spatial distribution of mobile ions) instead of mobile ion density or static ion dopants. The increase of C_{dl} originates from ion accumulation at the interface between the perovskite and the charge transport layer,[41] which can lead to the perovskite phase segregation, tuning of the band energy diagram, reduction of the free carrier lifetime and shielding of the built-in electric field, thus deteriorating device performance.[44–46] The processes involved in the degradation include the halide ion migration, organic cation migration, material decomposition, etc., with timescales of minutes, hours and days, respectively.[3,8] Since this work focuses on a reversible and

rapid decay process (*ca.* hours), we believe that the organic cation migration is dominant. Under the bias voltage aging conditions, the direction of the internal electric field is from the ETL to the HTL. Consequently, MA$^+$ ions accumulated at the HTL/perovskite and V$_{MA}^+$ ions at the ETL/perovskite (detailed discussion in ESI Section 2.2).†

Based on previous reports, the N_{ion} increase is related to the decrease of activation energy (E_a).[47,48] Non-stoichiometric perovskite can be generated due to phase segregation under the bias voltage conditions.[4] Namely, the molar ratio of I to Pb can change from ≥3 (lead-poor or lead-moderate phase) to <3 (lead-rich phase), leading to the lowered E_a of iodine vacancies and interstitial MA$^+$ as confirmed by the first-principles calculation.[49] According to the above discussion, we conclude that bias voltage mainly affects the accumulated mobile ions near the interface capacitance C_{dl} (namely the spatial distribution of mobile ions) which consequently leads to more captured free carriers and lower J_{sc}. Meanwhile, the mobile ion density increased moderately and the static ion dopant density remains almost unchanged.

2.3. Light-induced rapid degradation

Next, the rapid PCE degradation of the encapsulated devices under AM1.5G continuous illumination is studied. As shown in Fig. 4a–c, after 90 min storage under a light field, the PCEs of the reference, PEAI and PMMA devices decrease to only 67%, 83% and 80% of the initial values, respectively. The PCE loss primarily stems from the FF loss and the V_{oc} loss, although J_{sc} also dropped a little (3.76%, 1.61% and 2.45% for the reference, PEAI and PMMA devices) like in the voltage aging test. Both the

FF loss and the V_{oc} loss can be effectively suppressed by PMMA or PEAI, which agrees with previous research.[17,20,23] From the measured M–S results, the initial N of the three devices are calculated to be 1.28×10^{16}, 1.17×10^{16} and 1.05×10^{16} cm^{-3} for the reference, PEAI and PMMA devices, respectively. After the 90 min light soaking, the bulk doping densities of all devices only slightly increased to 1.46×10^{16} (14.0%↑), 1.30×10^{16} (11.1%↑), and 1.15×10^{16} (9.5%↑) cm^{-3} for the reference, PEAI and PMMA devices, respectively, implying no significant change in the concentration of static ions in the perovskite bulk. Aside from N, V_{bi} of the reference, PEAI and PMMA devices reduced by 83, 47 and 28 mV, respectively, which agrees with their corresponding V_{oc} loss. The apparent inhibition of V_{bi} and V_{oc} degradation by interface passivation indicates that the light-induced device degradation stems from the interface at the perovskite/carrier transport layer. In the following discussion based on the EIS results, we will show how the light field changes the interface properties and results in V_{oc} reduction.

The evolution of the EIS results in the Nyquist plots of the reference (a), PEAI (b) and PMMA (c) devices with increasing light soaking time (t_{light}) under AM1.5G continuous illumination and open-circuit conditions is characterized. Meanwhile, the corresponding fittings are displayed in Fig. 5d–f. From Fig. 5e, we observe that, with increasing t_{light}, the N_{ion} for the reference device increases significantly by 52%. These photo-induced mobile ions in the reference device result in the severe FF loss shown in Fig. 4 *via* non-radiative recombination.[42] In contrast, the increment ratios in the PMMA and the PEAI devices are only 28% and 34%, respectively. Compared with the reference device, the lower N_{ion} increase in the
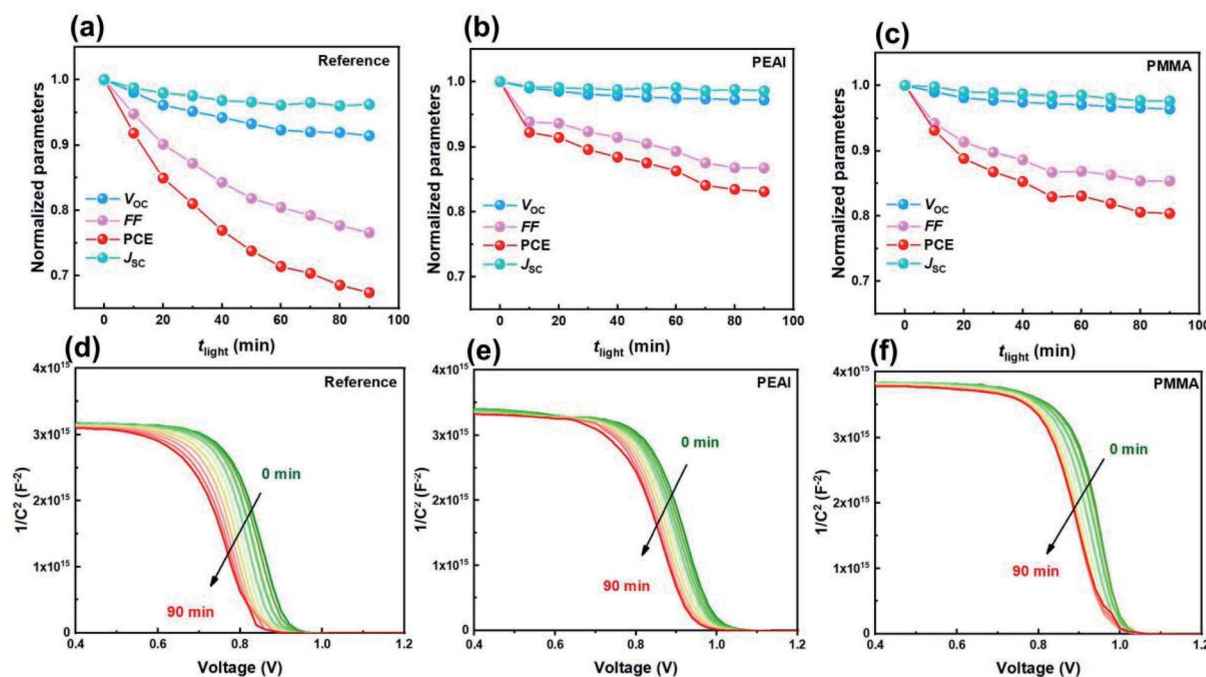

Fig. 4 Light-induced rapid degradation behavior of performance parameters of the encapsulated reference device (a), PEAI device (b) and PMMA device (c) with t_{light}, in the air at 25 °C. M–S plots of the degradation process over t_{light} of the reference device (d), PEAI device (e) and PMMA device (f) measured at 1 kHz and in the air at 25 °C.
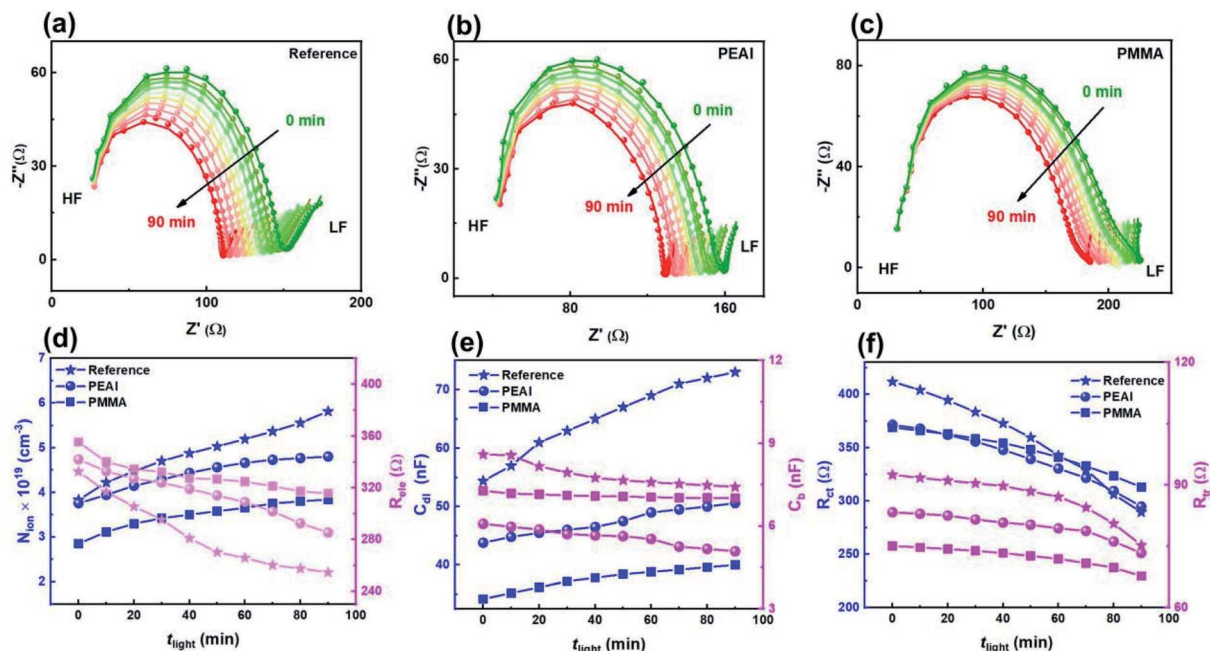
Fig. 5 Nyquist plots of the degradation process over t_{light} of the reference device (a), PEAI device (b) and PMMA device (c). The EIS measured using an AM1.5 solar simulator under the 0 V bias and at controlled temperature (25 °C). The symbols and solid lines represent the experiment data points and fitting curves, respectively. The fitting parameters of three devices with t_{light} from the equivalent circuit diagram ((d) for N_{ion} and R_{ele}, (e) for C_{dl} and C_b, and (f) for R_{ct} and R_{tr}).

modified devices proves that the PMMA or PEAI molecules efficiently suppress the conversion of lattice ions on the surface to mobile ions. This is because these passivation molecules tightly bind with the dangling bonds on the lattice surfaces and grain boundaries.[17,27,40,50,51] Consequently, the FF reduction of the passivated devices is largely suppressed. Meanwhile, the non-radiative recombination rate of free carriers is studied through analyzing the recombination resistance (R_{ele}).[40,52] As shown in Fig. 5d, with increasing t_{light}, the decrease in R_{ele} for the reference, PEAI and PMMA devices is 30.6%, 19.8% and 12.6%, respectively, indicating that the enhanced recombination probability of the reference is the highest among the three devices. In addition, like in the voltage aging test, the degradation of C_{dl} and R_{ct} may be the reasons for the slight J_{sc} drop. The 34% increase in C_{dl} for the reference device suggests a bad effect on free carrier transport at the interface, which leads to increased interfacial recombination, reflected by the decreased R_{ct} (shown in Fig. 5e). In contrast, when the perovskite was passivated by PEAI or PMMA, the variation of C_{dl} and R_{ct} became less than 10%. As shown in Fig. 5e and f, we notice that the variation of interface parameters (C_{dl}, R_{ct}) is greater than the variation of bulk parameters (C_b, R_{tr}) in both the modified and reference devices. Namely, aside from the interface accumulation observed in the voltage-aging test, the light field also increases N_{ion}, leading to a drop in FF and V_{oc}. Under the light aging conditions, the direction of the internal electric field is from the ETL to the HTL. Consequently, MA$^+$ ions accumulated at the HTL/perovskite and V$_{MA}^+$ ions at the ETL/perovskite (detailed discussion in ESI Section 2.2).† In addition, the PEAI- and PMMA-passivation layer can enhance their stability,

leading to slower degradation. Apart from suppression of the formation of charged defects at grain boundaries and surfaces as discussed above, PEAI and PMMA surface treatments can also increase the migration barrier of charged defects. For example, after the conventional 3D perovskite is modified with a 2D perovskite (PEA$_2$PbI$_4$), the migration barrier of ionic defects could increase from 0.680 eV to 0.905 eV, which thereby needs a much higher external field or much longer aging time.[53] Based on the above discussion, we consider that PMMA and PEAI modified layers can efficiently suppress ion migration, and consequently slow the performance degradation.

We notice that the PCE drop under the bias voltage aging test process is less significant than under the light aging test. The accelerated degradation under the light aging conditions can be ascribed to (1) phase separation, (2) excess free carriers, and (3) trap charging (neutral iodide).[54] Firstly, ion migration is one of the main causes of phase separation, which will result in PCE degradation. In this article, the N_{ion} in the bias voltage (dark) aging test is two orders of magnitude smaller than that in the light aging test which agrees with a previous report, in which the mobile ion density was related to light power.[23] Therefore, the phase separation induced degradation phenomenon in the light aging measurement process is more prominent than that under bias voltage aging conditions. Secondly, it has been reported that the excess holes and electrons reduce the E_a for ion migration within PSCs.[55] Compared to the bias voltage aging measurement, PSCs in the light aging measurement have a higher concentration of accumulated carriers and consequently lower E_a, resulting in the most severe phase separation.[44,45] Thirdly, the accumulated carriers can result in mobile

ions becoming trap charging states. For example, the interstitial iodide defect absorbs a free hole to form neutral iodide, which can accelerate the perovskite material's decomposition.[54] Based on the above discussion, we conclude that under the bias voltage aging test, the applied electric field mainly drives the preexisting mobile ion accumulation interface and maintains the preexisting mobile ion density. In contrast, under the light aging test, the applied light fields mainly increase the mobile ion density, which subsequently leads to more severe device degradation.

2.4. Heat-induced rapid degradation

The rapid degradation photovoltaic parameters of the encapsulated devices ((a) for the reference device, (b) for the PEAI device and (c) for the PMMA device) were examined at 85 °C using a thermo plate in the dark. As shown in Fig. 6, after the 90 min heating treatment, the PEAI and PMMA devices retain 79% and 84% of their initial values while the reference perovskite device retains only 74%. The PMMA device has the best stability; the photovoltaic parameters J_{sc}, V_{oc} and FF retain 92%, 97% and 94% of their initial values.

According to the Mott–Schottky relation (Fig. S7†), the calculated N is about 1.49×10^{16} cm^{-3} (2.59×10^{16} cm^{-3}, 73.8%↑ after heating treatment) for the reference device, 8×10^{15} cm^{-3} (1.32×10^{16} cm^{-3}, 65.0%↑) for the PEAI device and 7.6×10^{15} cm^{-3} (1.49×10^{16} cm^{-3}, 96.1%↑) for the PMMA device. Compared to the bias voltage and light aging experiment, after the 90 min heating treatment of the reference device, the relative increases of the static ion dopants in all three devices are significantly higher, regardless of passivation. Therefore, we consider that heat-induced degradation originates from the increased bulk doping densities, instead of interfacial degradation which dominates the bias voltage- or light-induced degradation.

Aside from the increased N, N_{ion} increases with t_{heat}, leading to the increase of C_{dl} (Fig. 6f). Like in voltage and light aging tests, the variation of N_{ion} and C_{dl} results in a reduced FF and J_{sc}. Although PEAI and PMMA can alleviate the variation of N_{ion} and C_{dl}, the performances of the three devices show obvious degradation. Meanwhile, the R_{ele} values of all three devices decrease as shown in Fig. 6e, implying a significantly increased capture probability of the free carriers in the three device types. Therefore, we consider that in the heat aging test, the PCE degradation is largely determined by the decomposition of the perovskite material itself. For example, deep level defects (e.g. metal Pb) could be formed during the decomposition process which could serve as recombination centers, leading to severely reduced FF and PCE.[11] In order to confirm the perovskite decomposition, the corresponding XRD experiments were conducted. Compared with light field treatment, the (220) orientation diffraction peaks of all devices are obviously weakened, and almost disappear after 90 min heat field treatment (Fig. S8†), implying more severe perovskite decomposition through volatilization of halide anions or the organic cation,[4,9,11] regardless of passivation. In addition, mobile ion migration into the electron/hole transport layer or metal electrode can cause failure of the corresponding functional layer, which will consequently lead to irreversible PCE degradation.[56,57] Therefore, during the heat aging process, the decomposition of
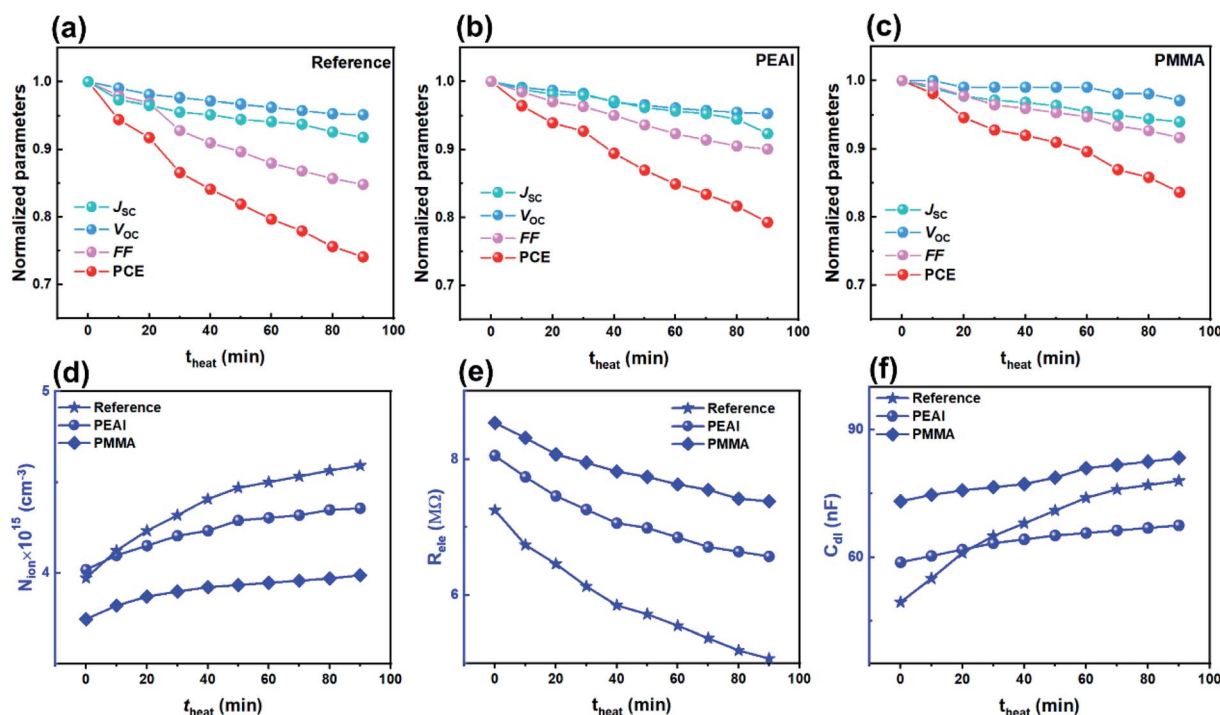

Fig. 6 Heat-induced rapid degradation behavior of performance parameters of the encapsulated reference device (a), PEAI device (b) and PMMA device (c) at 85 °C in the dark. Fitted values of the equivalent circuit components: (d) N_{ion}, (e) R_{ele}, and (f) C_{dl}.
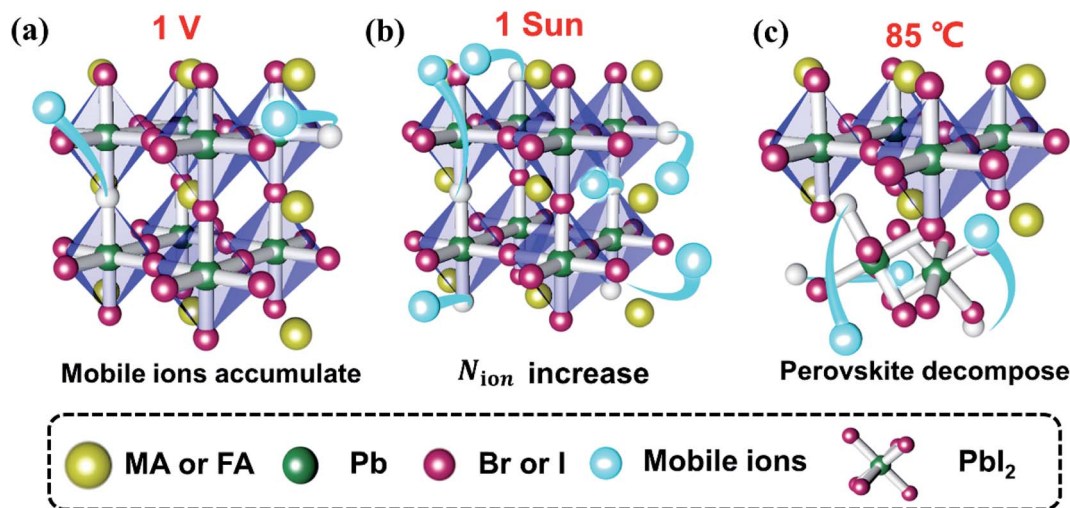
Fig. 7 Schematic of the effect of the external field on mobile ions under light (a), bias voltage (b) and heat conditions (c).

materials (including the perovskite and functional layer) should be responsible for the degradation of all devices' PCE, which is of distinct difference from the voltage and light aging tests.

In addition, the reason for the increase of N_{ion} under heating can also be ascribed to perovskite decomposition. It is well known that perovskite thermal decomposition can generate more voids or pinholes confirmed by scanning electron microscopy,[4] which results in a higher surface/volume ratio than in the fresh perovskite. Experiment and theory have proved that perovskites with a higher surface/volume ratio have a lower E_a than those with a smaller surface/volume ratio.[47,58] Consequently, under the heat aging process, the evolution of micromorphology is one of the reasons leading to the change of E_a, which leads to increased N_{ion}.

3. Conclusion

By comparing the three aging tests, we find that the bias voltage field is the least effective in facilitating device degradation while the light field and heat field are similarly effective. The light-induced and heat-induced degradation processes are both dominant with reduced FF while the voltage-induced degradation is dominant with reduced J_{sc}. The dominant mechanisms of the degradation under voltage, light and heat fields are different (Fig. 7). (a) The voltage field only results in accumulation of preexisting mobile ions near the interface; (b) the light field results in photo-induced mobile ions, leading to more severe mobile ion accumulation than in the voltage aging test; (c) the heat field results in material decomposition (including that of perovskite and functional layers). Through the comparison of the three types of device, we find that the polymer organic layer (PMMA) and low dimensional perovskite (PEAI) can efficiently suppress ion migration, especially the voltage and light-induced migration, which consequently improve the stability. However, the modified layer can't effectively alleviate the heat-induced degradation, which stems from perovskite decomposition. Therefore, to improve its thermal stability, it is

not only necessary to inhibit ion migration from the perspective of interface engineering, but also to enhance the E_a of ion migration of the material itself through component engineering.

Conflicts of interest

There are no conflicts to declare.

Acknowledgements

References

1 L. Meng, J. You and Y. Yang, *Nat. Commun.*, 2018, **9**, 1–4.
2 B. W. Park and S. I. Seok, *Adv. Mater.*, 2019, **31**, 1805337.
3 K. Domanski, B. Roose, T. Matsui, M. Saliba, S.-H. Turren-Cruz, J.-P. Correa-Baena, C. R. Carmona, G. Richardson, J. M. Foster, F. De Angelis, J. M. Ball, A. Petrozza, N. Mine, M. K. Nazeeruddin, W. Tress, M. Grätzel, U. Steiner, A. Hagfeldt and A. Abate, *Energy Environ. Sci.*, 2017, **10**, 604–613.
4 Y.-H. Lin, N. Sakai, P. Da, J. Wu, H. C. Sansom, A. J. Ramadan, S. Mahesh, J. Liu and R. D. Oliver, *Science*, 2020, **369**, 96–102.
5 J.-W. Lee, S.-G. Kim, J.-M. Yang, Y. Yang and N.-G. Park, *APL Mater.*, 2019, **7**, 041111.

6 R. Wang, M. Mujahid, Y. Duan, Z.-K. Wang, J. Xue and Y. Yang, *Adv. Funct. Mater.*, 2019, **29**, 1808843.

7 Y. Zhou and Y. Zhao, *Energy Environ. Sci.*, 2019, **12**, 1495–1511.

8 H. Wang, A. Guerrero, A. Bou, A. M. Al-Mayouf and J. Bisquert, *Energy Environ. Sci.*, 2019, **12**, 2054–2079.

9 D. B. Khadka, Y. Shirai, M. Yanagida and K. Miyano, *J. Mater. Chem. C*, 2018, **6**, 162–170.

10 S. N. Raja, Y. Bekenstein, M. A. Koc, S. Fischer, D. Zhang, L. Lin, R. O. Ritchie, P. Yang and A. P. Alivisatos, *ACS Appl. Mater. Interfaces*, 2016, **8**, 35523–35533.

11 N. Li, Y. Luo, Z. Chen, X. Niu, X. Zhang, J. Lu, R. Kumar, J. Jiang, H. Liu, X. Guo, B. Lai, G. Brocks, Q. Chen, S. Tao, D. P. Fenning and H. Zhou, *Joule*, 2020, **4**, 1743–1758.

12 S. T. Birkhold, J. T. Precht, R. Giridharagopal, G. E. Eperon, L. Schmidt-Mende and D. S. Ginger, *J. Phys. Chem. C*, 2018, **122**, 12633–12639.

13 G. Divitini, S. Cacovich, F. Matteocci, L. Cinà, A. Di Carlo and C. Ducati, *Nat. Energy*, 2016, **1**, 1–6.

14 W. Chen, W. Li, Z. Gan, Y.-B. Cheng, B. Jia and X. Wen, *Chem. Mater.*, 2019, **31**, 9049–9056.

15 G. Xia, B. Huang, Y. Zhang, X. Zhao, C. Wang, C. Jia, J. Zhao, W. Chen and J. Li, *Adv. Mater.*, 2019, **31**, 1902870.

16 W. Fu, H. Liu, X. Shi, L. Zuo, X. Li and A. K. Y. Jen, *Adv. Funct. Mater.*, 2019, **29**, 1900221.

17 Q. Jiang, Y. Zhao, X. Zhang, X. Yang, Y. Chen, Z. Chu, Q. Ye, X. Li, Z. Yin and J. You, *Nat. Photonics*, 2019, **13**, 460–466.

18 D. S. Lee, J. S. Yun, J. Kim, A. M. Soufiani, S. Chen, Y. Cho, X. Deng, J. Seidel, S. Lim, S. Huang and A. W. Y. Ho-Baillie, *ACS Energy Lett.*, 2018, **3**, 647–654.

19 Y. Liu, S. Akin, L. Pan, R. A. Uchida, N. Arora, J. V. H. Milić, A. Hinderhofer, F. Schreiber, A. R. Z. Uhl, S. M. Zakeeruddin, A. D. Hagfeldt, M. Ibrahim and M. Grätze, *Sci. Adv.*, 2019, **5**, eaaw2543.

20 S. Kundu and T. L. Kelly, *Mater. Chem. Front.*, 2018, **2**, 81–89.

21 A. A. Maxim, S. N. Sadyk, D. Aidarkhanov, C. Surya, A. Ng, Y. H. Hwang, T. S. Atabaev and A. N. Jumabekov, *Nanomaterials*, 2020, **10**, 291.

22 M. Fischer, K. Tvingstedt, A. Baumann and V. Dyakonov, *ACS Appl. Energy Mater.*, 2018, **1**, 5129–5134.

23 X. Chen, Y. Shirai, M. Yanagida and K. Miyano, *J. Phys. Chem. C*, 2019, **123**, 3968–3978.

24 Y. Feng, J. Bian, S. Wang, C. Zhang, M. Wang and Y. Shi, *J. Mater. Chem. C*, 2019, **7**, 8294–8302.

25 I. Zarazua, G. Han, P. P. Boix, S. Mhaisalkar, F. Fabregat-Santiago, I. Mora-Sero, J. Bisquert and G. Garcia-Belmonte, *J. Phys. Chem. Lett.*, 2016, **7**, 5105–5113.

26 N. A. Nadege Ouedraogo, M. Yang, C. He, Y. Chen, X. Zhang, H. Yan, C. B. Han and Y. Zhang, *Sustainable Energy Fuels*, 2020, **4**, 4257–4263.

27 Y. Chen, Q. Meng, Y. Xiao, X. Zhang, J. Sun, C. B. Han, H. Gao, Y. Zhang, Y. Lu and H. Yan, *ACS Appl. Mater. Interfaces*, 2019, **11**, 44101–44108.

28 E. Aydin, M. De Bastiani and S. De Wolf, *Adv. Mater.*, 2019, **31**(25), e1900428.

29 B. Chen, P. N. Rudd, S. Yang, Y. Yuan and J. Huang, *Chem. Soc. Rev.*, 2019, **48**, 3842–3867.

30 E. Bi, W. Tang, H. Chen, Y. Wang, J. Barbaud, T. Wu, W. Kong, P. Tu, H. Zhu, X. Zeng, J. He, S.-I. Kan, X. Yang, M. Grätzel and L. Han, *Joule*, 2019, 2748–2760.

31 O. Hentz, A. Singh, Z. Zhao and S. Gradečak, *Small Methods*, 2019, **3**, 1900110.

32 W. Jiang, J. Ying, W. Zhou, K. Shen, X. Liu, X. Gao, F. Guo, Y. Gao and T. Yang, *Chem. Phys. Lett.*, 2016, **658**, 71–75.

33 W. Li, W. Zhang, S. Van Reenen, R. J. Sutton, J. Fan, A. A. Haghighirad, M. B. Johnston, L. Wang and H. J. Snaith, *Energy Environ. Sci.*, 2016, **9**, 490–498.

34 Y. Lin, Y. Bai, Y. Fang, Z. Chen, S. Yang, X. Zheng, S. Tang, Y. Liu, J. Zhao and J. Huang, *J. Phys. Chem. Lett.*, 2018, **9**, 654–658.

35 Y. Lin, Y. Bai, Y. Fang, Q. Wang, Y. Deng and J. Huang, *ACS Energy Lett.*, 2017, **2**, 1571–1572.

36 S. G. Motti, D. Meggiolaro, S. Martani, R. Sorrentino, A. J. Barker, F. De Angelis and A. Petrozza, *Adv. Mater.*, 2019, **31**, 1901183.

37 J. Wu, J. Shi, Y. Li, H. Li, H. Wu, Y. Luo, D. Li and Q. Meng, *Adv. Energy Mater.*, 2019, **9**, 1901352.

38 U. T. Ravishankar Sandheep and K. Thomas, *Science*, 2021, **371**, 6484.

39 L. Fu, H. Li, L. Wang, R. Yin, B. Li and L. Yin, *Energy Environ. Sci.*, 2020, **13**, 4017–4056.

40 E. C. Smith, C. L. C. Ellis, H. Javaid, L. A. Renna, Y. Liu, T. P. Russell, M. Bag and D. Venkataraman, *J. Phys. Chem. C*, 2018, **122**, 13986–13994.

41 C. Aranda, J. Bisquert and A. Guerrero, *J. Chem. Phys.*, 2019, **151**, 124201.

42 H. Chen, X. Wen, R. S. Sheng, S. Huang, X. Deng, M. A. Green and A. Ho-Baillie, *ACS Appl. Mater. Interfaces*, 2016, **8**, 5351–5357.

43 G. H. Isaac Zarazua, P. P. Boix, S. Mhaisalkar, F. Fabregat-Santiago, I. Mora-Seró, J. Bisquert and G. Garcia-Belmonte, *J. Phys. Chem. Lett.*, 2016, **7**, 5105–5113.

44 T.-Y. Zhu and D.-J. Shu, *J. Phys. Chem. C*, 2019, **123**, 5312–5320.

45 L. Bertoluzzi, C. C. Boyd, N. Rolston, J. Xu, R. Prasanna, B. C. O'regan and M. D. Mcgehee, *Joule*, 2019, **4**, 109–127.

46 D. Moia, I. Gelmetti, P. Calado, W. Fisher, M. Stringer, O. Game, Y. Hu, P. Docampo, D. Lidzey, E. Palomares, J. Nelson and P. R. F. Barnes, *Energy Environ. Sci.*, 2019, **12**, 1296–1308.

47 D. Meggiolaro, E. Mosconi and F. D. Angelis, *ACS Energy Lett.*, 2019, **4**, 779–785.

48 J. M. Azpiroz, E. Mosconi, J. Bisquert and F. D. Angelis, *Energy Environ. Sci.*, 2015, **8**, 2118–2127.

49 W. Yin, T. Shi and Y. Yan, *Appl. Phys. Lett.*, 2014, **104**, 063903.

50 J. Yang, C. Liu, C. Cai, X. Hu, Z. Huang, X. Duan, X. Meng, Z. Yuan, L. Tan and Y. Chen, *Adv. Energy Mater.*, 2019, 1970064.

51 E. C. Smith, C. L. C. Ellis, H. Javaid, B. G. Arden and D. Venkataraman, *Phys. Chem. Chem. Phys.*, 2019, **21**, 20720–20726.

52 M. N. F. Hoque, N. Islam, Z. Li, G. Ren, K. Zhu and Z. Fan, *ChemSusChem*, 2016, **9**, 2692–2698.

53 C. Chen, Z. Song, C. Xiao, R. A. Awni, C. Yao, N. Shrestha, C. Li, S. S. Bista, Y. Zhang, L. Chen, R. J. Ellingson, C.-S. Jiang, M. Al-Jassim, G. Fang and Y. Yan, *ACS Energy Lett.*, 2020, **5**, 2560–2568.

54 V. K. Mark, K. M. Anoop, A. K. Eugene and V.-F. Iris, *Energy Environ. Sci.*, 2019, **12**, 550–558.

55 Y. Lin, B. Chen, Y. Fang, J. Zhao, C. Bao, Z. Yu, Y. Deng, P. N. Rudd, Y. Yan, Y. Yuan and J. Huang, *Nat. Commun.*, 2018, **9**, 1–9.

56 M.-W. An, Z. Xing, B.-S. Wu, F.-F. Xie, S.-Y. Zheng, L.-L. Deng, X. Wang, B.-W. Chen, D.-Q. Yun, S.-Y. Xie, R.-B. Huang and L.-S. Zheng, *Rare Met.*, 2020, **40**, 1691–1697.

57 K. Domanski, J.-P. Correa-Baena, N. Mine, M. K. Nazeeruddin, A. Abate, M. Saliba, W. Tress, A. Hagfeldt and M. Grätzel, *ACS Nano*, 2016, **10**, 6306–6314.

58 J. Xing, Q. Wang, Q. Dong, Y. Yuan, Y. Fang and J. Huang, *Phys. Chem. Chem. Phys.*, 2016, **18**, 30484–30490.